

Improving the applicability of the Pauli kinetic energy density based semilocal functional for solids

Subrata Jana,^{1,*} Sushant Kumar Behera,^{1,†} Szymon Śmiga,^{2,‡} Lucian A. Constantin,^{3,§} and Prasanjit Samal^{1,¶}

¹*School of Physical Sciences, National Institute of Science Education and Research, HBNI, Bhubaneswar 752050, India*

²*Institute of Physics, Faculty of Physics, Astronomy and Informatics,
Nicolaus Copernicus University, Grudziadzka 5, 87-100 Toruń, Poland*

³*Istituto di Nanoscienze, Consiglio Nazionale delle Ricerche CNR-NANO, 41125 Modena, Italy*

(Dated: April 23, 2021)

The Pauli kinetic energy enhancement factor $\alpha = (\tau - \tau^W)/\tau^{unif}$ is an important density ingredient, used to construct many meta-generalized gradient approximations (meta-GGA) exchange-correlation (XC) energy functionals, including the very successful strongly constrained and appropriately normed (SCAN) semilocal functional. Another meta-GGA functional, known as MGGAC [Phys. Rev. B 100, 155140 (2019)], is also proposed in recent time depending only on the α ingredient and based on the generalization of the Becke-Roussel approach with the cusplless hydrogen exchange hole density. The MGGAC functional is proved to be a very useful and competitive meta-GGA semilocal functional for electronic structure properties of solids and molecules. Based on the successful implication of the ingredient α , which is also useful to construct the one-electron self-interaction free correlation energy functional, here we propose revised correlation energy for MGGAC exchange functional which is more accurate and robust, especially for the high and low-density limits of the uniform density scaling. The present XC functional, named as revised MGGAC (rMGGAC), shows an impressive improvement for the structural and energetic properties of solids compared to its previous version. Moreover, the assessment of the present constructed functional shows to be quite useful in solid-state physics in terms of addressing several current challenging solid-state problems.

I. INTRODUCTION

The Kohn-Sham (KS) density functional theory (DFT)¹ has become an indispensable computational framework for performing the electronic structure calculations of new generation electronic devices²⁻⁴, energy storage devices⁵, catalyst⁶ and spintronics devices⁷⁻⁹. Despite the extraordinary potential and considerable progress made to date, challenges remain to bridge the gap between simulations and experimental findings. Efforts have increased in developing new strategies in understanding the theory and practical implementation of complex systems, but current progress is still far from sufficient. However, recent strategies of the development of non-empirical exchange-correlation (XC) functionals by satisfying quantum mechanical exact constraints¹⁰ exhibit extremely prosperous to catch the interplay of dimensionality, correlation, charge, orbital character, topological, and other large reservoirs of exotic properties of condensed matter systems¹¹.

Within the exact quantum constraints, we recall coordinate transformations and density scaling rules of XC functionals¹²⁻¹⁵, second (and fourth) order gradient expansion of XC energies¹⁶⁻²¹, low and high density limits of the correlation energy functional²²⁻²⁴, correct asymptotic behavior of the XC energy density²⁵⁻³⁰ or potential^{26,31-39}, quasi-2D limit of the XC energy⁴⁰⁻⁴³, and exact properties of the XC hole⁴⁴⁻⁴⁷. All these constraints are taken into care in different rungs (recognized as the Jacob Ladder⁴⁸) of the semilocal density functionals approximations (DFA) starting from the local density approximation (LDA)⁴⁹, throughout generalization gra-

dient approximation (GGA)⁵⁰⁻⁶³ to meta-generalization gradient approximation (meta-GGA)^{10,34,44,64-84}. The recent trends in DFT showed that the latter family of DFAs can offer unprecedented performance, becoming the most auspicious choice of doing both the quantum chemical and material simulations^{44,85-112}.

We recall that the meta-GGA XC energy functionals have the general form

$$E_{xc}[\rho_{\uparrow}, \rho_{\downarrow}] = \int d\mathbf{r} \rho(\mathbf{r}) \epsilon_{xc}^{LDA} F_{xc}(\rho_{\uparrow}, \rho_{\downarrow}, \nabla\rho_{\uparrow}, \nabla\rho_{\downarrow}, \tau_{\uparrow}, \tau_{\downarrow}), \quad (1)$$

where ϵ_{xc}^{LDA} is the LDA XC energy per particle, F_{xc} is the XC enhancement factor, and ρ_{σ} and τ_{σ} are the σ -spin density and kinetic energy density, respectively. Eq. (1) is quite flexible, being able to recognize covalent, metallic, and weak bonds¹¹³. Moreover, the utilization of KS kinetic energy density ($\tau(\mathbf{r}) = \frac{1}{2} \sum_{i,\sigma} |\nabla\psi_{i,\sigma}|^2$, $\tau = \tau_{\uparrow} + \tau_{\downarrow}$) and different ingredients built in from $\tau(\mathbf{r})$, density ($\rho = \rho_{\uparrow} + \rho_{\downarrow}$), and gradient of density ($\nabla\rho$) allow to recover important exact conditions of the XC functional^{10,34,114}. Among them, we recall $\alpha = (\tau - \tau^W)/\tau^{unif}$, also known as the Pauli kinetic energy¹¹⁵⁻¹¹⁹ enhancement factor (F_s^{θ}), is used to construct several modern XC functionals^{10,72,113,120,121}. Here $\tau^W = |\nabla\rho|^2/(8\rho)$ and $\tau^{unif} = (3/10)(3\pi^2)^{2/3} \rho^{5/3}$ are the von Weizsäcker and Thomas-Fermi kinetic energy densities, respectively.

The α ingredient helps to impose some exact constraints in the functional form, such as the strongly tightened bound of exchange, i.e. $F_x \leq 1.174^{10,122,123}$. Importantly, this allows a negative slope ($\partial F_x/\partial\alpha \leq 0$) which is related to an improvement in the prediction

of the band gap⁸⁴. Also, the use of solely α and $s = |\nabla\rho|/[2(3\pi^2)^{1/3}\rho^{4/3}]$ (reduced density gradient) makes the meta-GGA XC functional free from the order-of-limit anomaly, that is important for the structural phase transition pressures and energies^{73,124}. Focusing on the XC functional development, a popular non-empirical meta-GGA XC functional is the Strongly Constrained and Appropriately Normed (SCAN)¹⁰ semilocal DFA. Besides the SCAN, it was also recently proposed the MGGAC XC functional⁸⁰, whose exchange part depends only on the α ingredient, being developed from a generalization of the Becke-Roussel approach^{78,125}, and using the cusplless hydrogen model for the exchange hole density. The MGGAC functional showed its productive power over other meta-GGAs in terms of the band gap performance for bulk solids¹²⁶, two dimensional (2D) van der Waals (vdW) materials^{2,3,126}, and structural phase stability of solids¹²⁷.

The MGGAC exchange enhancement factor is a simple monotonic function of α and satisfies (i) the strongly tightened bound of exchange $F_x \leq 1.174$ ($F_x = 1.174$ for two-electron systems), (ii) the uniform electron gas limit ($F_x = 1$) when $\alpha = 1$, and (iii) the cusplless hydrogen related behavior ($F_x = 0.937$) at $\alpha \rightarrow \infty$. On the other hand, the MGGAC correlation energy functional is based on the GGA PBE correlation form¹²⁸, where the linear response parameter ($\beta(r_s) = 0.030$) was fitted to the equilibrium lattice constants of several bulk solids. Then, it is not one-electron self-interaction free, an important constraint that should be satisfied by every meta-GGA functional. Nevertheless, the MGGAC DFA has demonstrated several successes which include (i) improved thermochemical properties⁸⁰, (ii) improved fundamental band gap for bulk and layer solids¹²⁶, and (iii) correct energy ordering for challenging polymorphs of solids¹²⁷. However, the functional has its own limitations such as moderate performance for lattice constants, bulk moduli, and cohesive energies for bulk solids⁸⁰. Therefore, it is desirable to improve the accessibility of the MGGAC functional for solids by removing some deficiencies of the current version. In order to do so, we keep the MGGAC exchange unchanged, modifying only the correlation part of DFA energy such that it becomes exact for one electron densities and more robust for low- and high- density limits.

The paper is organized as follows: in the next section, we will construct the revised MGGAC correlation energy functional dependent on both α and s . Later, we will couple the proposed correlation with the MGGAC exchange to assess the functional performance for molecular and solid-state properties. Furthermore, we also investigate the low- and high- density limit of the XC functional. Lastly, we summarize our findings.

II. CORRELATION FUNCTIONAL CONSTRUCTION

In this section, we propose the revised MGGAC (rMGGAC) correlation energy functional. The rMGGAC correlation functional is constructed by incorporating the following important constraints: (i) self-interaction free for one-electron systems; (ii) accurate for two electron systems; (iii) accurate for slowly varying densities; and (iv) accurate spin-dependence in the low-density or strong-interaction limit. While constraint (iii) is satisfied by the MGGAC correlation energy functional⁸⁰ (i.e., from the PBE form), conditions (i), (ii), and (iv) are not. To achieve this goal, we propose the rMGGAC correlation functional, dependent on α and s such as,

$$\epsilon_c^{rMGGAC} = \epsilon_c^0 f_1(\alpha, s) + \epsilon_c^1 f_2(\alpha, s), \quad (2)$$

where

$$\begin{aligned} \epsilon_c^1 &= \epsilon_c^{LSDA1} + H_1 \\ \epsilon_c^0 &= (\epsilon_c^{LDA0} + H_0)G_c(\zeta). \end{aligned} \quad (3)$$

Here, ϵ_c^{LSDA1} is the Perdew-Wang 1992 (PW92) LSDA correlation⁴⁹, and $\epsilon_c^{LDA0}G_c(\zeta)$ is the local correlation from SCAN functional¹⁰, that has been shown to be accurate for two electron systems^{10,129}. Here $\zeta = (\rho_\uparrow - \rho_\downarrow)/\rho$ is the relative spin polarization. Note that it does not contain the gradient of the density, having the following expressions¹⁰

$$\epsilon_c^{LDA0} = -b_{1c}/(1 + b_{2c}r_s^{1/2} + b_{3c}r_s), \quad (4)$$

and

$$G_c(\zeta) = \{1 - 2.3631[d_x(\zeta) - 1]\}(1 - \zeta^{12}), \quad (5)$$

$$d_x(\zeta) = [(1 + \zeta)^{4/3} + (1 - \zeta)^{4/3}]/2. \quad (6)$$

Here, we utilize $H_0 = b_{1c} \ln[1 + w_0(1 - g_\infty(\zeta = 0, s))]$ and $H_1 = \gamma\phi^3 \ln[1 + w_1(1 - g(At^2))]$ ¹⁰, with $w_0 = \exp[-\epsilon_c^{LDA0}/b_{1c}] - 1$, $g_\infty = 1/(1 + 4\chi_\infty(\zeta = 0)s^2)^{1/4}$, $w_1 = \exp[-\epsilon_c^{LDA1}/(\gamma\phi^3)] - 1$, $g(At^2) = 1/(1 + At^2)^{1/4}$, $A = \beta/(\gamma w_1)$, and $t = (3\pi^2/16)^{1/3}s/(\phi r_s^{1/2})$ (a reduced density gradient for correlation) from SCAN correlation¹⁰. The used terms and parameters are as follows: $b_{1c} = 0.0285764$, $b_{2c} = 0.0889$, $b_{3c} = 0.125541$, $g_\infty(\zeta = 0, s) = 1/(1 + 4\chi_\infty(\zeta = 0)s^2)^{1/4}$, $\chi_\infty(\zeta = 0) = 0.128026$, $\gamma = 0.031091$, and $\phi = [(1 + \zeta)^{2/3} + (1 - \zeta)^{2/3}]/2$. The readers are suggested to go through the supporting information of ref.¹⁰ for details of the terms and parameters values constructed. We use $\beta = 0.066725$, which is the correct second-order coefficient in the high-density limit, also present in PBE correlation⁵⁴.

Finally, we construct the functions $f_1(\alpha, s)$ and $f_2(\alpha, s)$, from the following conditions:

(i) For the slowly varying density limit, which is recognized as $\alpha \approx 1$ and $s \approx 0$, ϵ_c^{rMGGAC} becomes ϵ_c^1 .

(ii) For one electron or two electron singlet state, which is recognized as $\alpha \approx 0$, ϵ_c^{rMGGAC} becomes ϵ_c^0 .

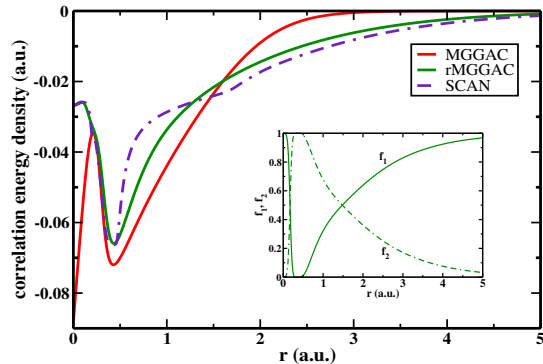


FIG. 1. Correlation energy per particle ϵ_c versus the radial distance r , for Ne atom. In the inset we show the functions f_1 and f_2 .

To satisfy these two conditions, we propose following ansatz

$$f_2(\alpha, s) = \frac{3[g(\alpha, s)]^3}{1+[g(\alpha, s)]^3+[g(\alpha, s)]^6} \quad (7)$$

$$f_1(\alpha, s) = 1 - f_2, \quad (8)$$

$$(9)$$

where

$$g(\alpha, s) = \frac{(1 + \gamma_1)\alpha}{\gamma_1 + \alpha + \gamma_2 s^2}. \quad (10)$$

The parameters $\gamma_1 = 0.08$ and $\gamma_2 = 0.3$ are chosen from the atomization energies of the AE6 molecules¹³⁰. Note that in the tail of the density, if the valence atomic orbital is degenerate, as in the case of Ne atom, then $\alpha \rightarrow \infty$, else $\alpha \rightarrow 0$ as in case of alkali and alkaline-earth atoms.

In Fig. 1 we show a comparison between rMGGAC, MGGAC and SCAN correlation energies per particle, for Ne atom. By construction, rMGGAC recovers ϵ_c^0 at the nucleus (where $\alpha \approx 0$) and in the tail of the density (where s diverges), while it recovers ϵ_c^1 in the atomic core (where the density is compact and slowly-varying). Overall, rMGGAC agrees closely with, but is smoother than SCAN, being significantly different from the MGGAC behavior.

We mention that the choice of the $f_1(\alpha, s)$, $f_2(\alpha, s)$, and ϵ_c^{rMGGAC} keeps the correct constraint of the correlation energy functional. Such as, in the rapidly varying density limit, recognized as $t \rightarrow \infty$ and $s \rightarrow \infty$, both H_0 and H_1 correctly cancel with ϵ_c^{LSDA0} and ϵ_c^{LSDA1} , respectively, making the correlation vanishes, an important constraint satisfied by all functionals constructed on the top of PBE form⁵⁴. Nevertheless, as shown in Fig. 1, this vanishing process is much slower for rMGGAC and SCAN than for MGGAC. Here we also note that in the tail of the density, if the valence atomic orbital is degenerate, as in the case of Ne atom, then $\alpha \rightarrow \infty$, else $\alpha \rightarrow 0$ as in case of alkali and alkaline-earth atoms.

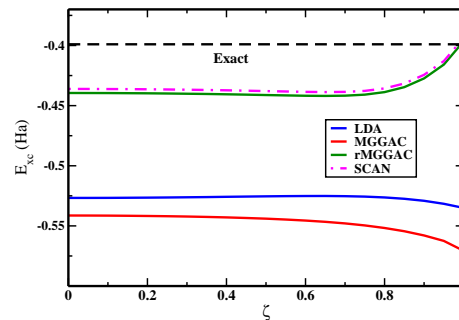


FIG. 2. Exchange-correlation energy in the low-density limit for spin-polarized one electron Gaussian density.

TABLE I. Error statistics (mean absolute error (MAE) and mean absolute relative error (MARE)) of the correlation energy per electron (E_c/N in mHa) for 25 atoms and ions. Full results are reported in Ref.¹³².

Error	SCAN	MGGAC	rMGGAC
MAE	3.7	10.5	3.4
MARE ^a	11.3	48.5	11.0

a) computed without the H atom.

In the low-density limit (see APPENDIX A for details), the rMGGAC XC energy functional becomes independent of ζ for $0 \leq \zeta \leq 0.7$ (as shown in Fig. 2 for one electron Gaussian density). The ζ independence of the XC functional is an important constraint not only for Wigner crystals, but also for the atomization energies¹³¹.

To quantify the performance of correlation functional for high-density limit, in Table I, we consider the correlation energies for the benchmark test of several atoms and ions, also used in Ref.¹³³. It is shown that the rMGGAC correlation energy considerably improves over MGGAC, being in line with the SCAN correlation.

Finally in Fig. 3 we compare the SCAN, MGGAC, and rMGGAC XC enhancement factors $F_{xc}(\zeta, \alpha, s, r_s)$, for the spin-unpolarized choice ($\zeta = 0$) and $\alpha = 0$ (that is describing the two-electron singlet states) and $\alpha = 1$ (the case of slowly-varying density limit when $s \leq 1$). In both panels, the $r_s = 0$ represents the exchange-only (high-density) limit, and we observe that MGGAC (rMGGAC) enhancement factor is independent on s ($F_x^{MGGAC} = 1.174$ for $\alpha = 0$, and $F_x^{MGGAC} = 1$ for $\alpha = 1$). Overall, the rMGGAC XC enhancement factor is slightly bigger than SCAN for $\alpha = 0$, and slightly smaller than SCAN $\alpha = 1$. We also note the large differences between MGGAC and rMGGAC, especially for the low-density cases ($r_s = 10$).

III. RESULTS AND DISCUSSIONS

In this section, we present the assessment of the performance of the rMGGAC XC DFA, along with SCAN and

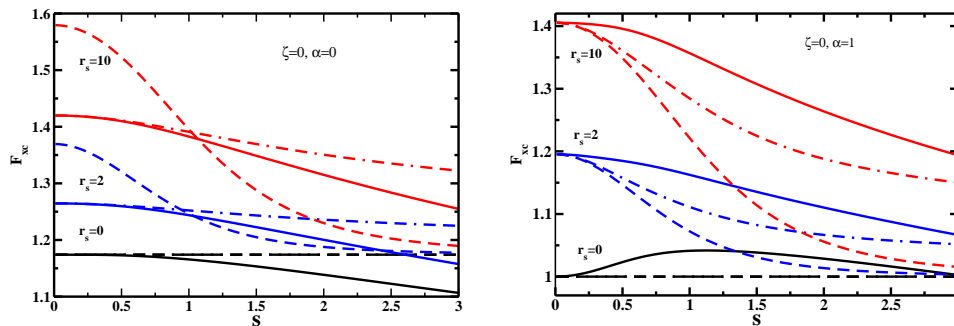


FIG. 3. Shown is the F_{xc} versus the reduced gradient s , for SCAN (solid), MGGAC (dashed), and rMGGAC (dashed-dotted) functionals, considering $\zeta = 0, \alpha = 0$ (upper panel) and $\zeta = 0, \alpha = 1$ (lower panel), and several values of the bulk parameter ($r_s = 0, 2$, and 10).

TABLE II. The test set of 41 solids considered in this work for lattice constants, bulk moduli, and cohesive energies. The space group is indicated in parenthesis.

Solids for lattice constants, bulk moduli, and cohesive energies
Li ($Im\bar{3}m$), Na ($Im\bar{3}m$), Ca ($Fm\bar{3}m$), Sr ($Fm\bar{3}m$), Ba ($Im\bar{3}m$), Al ($Fm\bar{3}m$), Cu ($Fm\bar{3}m$), Rh ($Fm\bar{3}m$), Pd ($Fm\bar{3}m$), Ag ($Fm\bar{3}m$), Au ($Fm\bar{3}m$), Cs ($Im\bar{3}m$), Fe ($Im\bar{3}m$), Ir ($Fm\bar{3}m$), K ($Im\bar{3}m$), Mo ($Im\bar{3}m$), Nb ($Im\bar{3}m$), Ni ($Fm\bar{3}m$), Pt ($Fm\bar{3}m$), Rb ($Im\bar{3}m$), Ta ($Im\bar{3}m$), V ($Im\bar{3}m$), W ($Im\bar{3}m$), C ($Fd\bar{3}m$), Si ($Fd\bar{3}m$), Ge ($Fd\bar{3}m$), SiC ($F\bar{4}3m$), GaAs ($F\bar{4}3m$), AlAs ($F\bar{4}3m$), AlN ($F\bar{4}3m$), AlP ($F\bar{4}3m$), GaN ($F\bar{4}3m$), GaP ($F\bar{4}3m$), InAs ($F\bar{4}3m$), InP ($F\bar{4}3m$), InSb ($F\bar{4}3m$), LiF ($Fm\bar{3}m$), LiCl ($Fm\bar{3}m$), NaF ($Fm\bar{3}m$), NaCl ($Fm\bar{3}m$), MgO ($Fm\bar{3}m$)

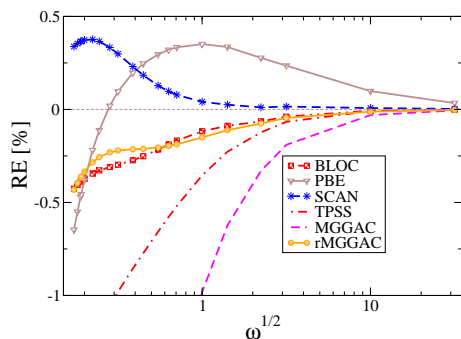


FIG. 4. Relative error on total energies of harmonium atoms for various values of confinement strength ω .

MGGAC methods for harmonium atom, various molecular and solid-state problems including the band gap assessment and structural phase transition of challenging systems.

A. Model system: Harmonium atom

We have tested the performance of the several DFAs (including the rMGGAC) against the harmonium atom¹³⁵, for various values of the confinement strength ω . We recall, that at small values of ω , the system is strongly correlated, whereas for large values of ω it is tightly bounded. These two regimes are very important for many condensed matter applications. Hence, the harmonium atom provides an excellent tool for testing ap-

proximate density functional methods^{136,137}. Similarly to our past studies^{138,139}, in order to perform calculations we have utilized an even-tempered Gaussian basis set from Ref. 140 for $\omega \in [0.03, 1000]$. As a reference results, we have used full configuration interaction (FCI) data obtained in the same basis set which have been proved to be close to exact values¹³⁸.

In Fig. 4, we report the relative error (RE) on total energies calculated with respect to reference data for several XC functionals as a function of ω . All DFAs energies have been obtained in post-SCF fashion on top of self-interaction free OEPx (optimized effective potential exact exchange) densities as in Refs. 138 and 139. One can note the remarkable good performance of rMGGAC functional along with the whole range of ω with an overall MARE of 0.21%. Moreover, rMGGAC significantly outperforms the MGGAC (MARE=2.67%), being especially visible for the strongly correlated regime. This may indicate that the new correlation functional form is more compatible with MGGAC exchange. The rMGGAC behavior is also quite similar to BLOC functional¹⁴¹ which also underestimate slightly the reference results with an overall MARE of 0.23%. The SCAN DFA gives similar results (MARE=0.20%), although in this case, we observe the overestimation. For comparison, we also show the TPSS and PBE data which gives an overall MARE of 0.78% and 0.28%, respectively.

TABLE III. The error statistics (MAEs and MAREs) of equilibrium lattice constants (LC) (a_0 in mÅ), bulk modulus (BM) (B_0 in GPa), and cohesive energies (COH) (ϵ_{coh} in eV/atom) of 41 solids. For band gaps (ϵ_g) we consider 40 bulk semiconductors which includes the 31 semiconducting systems band gaps from SBG31 test of Ref.¹³⁴ and additionally we include the band gaps of 9 solids (Cu₂O, CuBr, ScN, SnTe, MgC NaCl, LiCl, NaF, and LiF). The MARE of the SBG31 test is also reported. For Surface energies ($\epsilon_{\text{surface}}$ in J/m²) we consider the (111) surface. We also calculate the CO molecule adsorption energies (ϵ_{ads}) on top of the (111) surface (in eV). For both cases we consider five different transition metals taken from Ref.⁸⁰. The SCAN values are taken from Ref.¹⁰⁹. The surface energies and adsorption energies of SCAN and MGGAC functionals are taken from ref.⁸⁰. The LC20, BM20, COH20, and SBG31 test sets results of MGGAC are taken from ref.⁸⁰. See ref.¹³² for the details of the rMGGAC values.

	SCAN	MGGAC	rMGGAC
Lattice constants			
MAE (mÅ)	38	51	38
MARE (%)	0.81	1.09	0.81
MAE of LC20 (mÅ)	25	45	30
Bulk moduli			
MAE (GPa)	7.5	11.5	8.5
MARE (%)	6.3	11.2	8.8
MAE of BM20 (GPa)	4.2	10.0	4.6
Cohesive energies			
MAE (eV/atom)	0.19	0.36	0.30
MARE (%)	4.80	9.29	8.11
MAE of COH20 (eV/atom)	0.11	0.38	0.27
Band gaps			
MAE (eV)	1.1	0.8	0.5
MARE (%)	39.2	40.6	43.3
SBG31	38.1	40.7	42.6
Surface energies			
MAE (eV)	0.48	0.21	0.27
MARE (%)	22.8	10.5	12.2
Adsorption energies			
MAE (J/m ²)	0.51	0.28	0.31
MARE (%)	42.1	23.7	24.3

B. General assessment for solids

For general assessment, we first consider the 41 bulk solids set proposed in Table II and we compute the equilibrium lattice constants (LC41), bulk moduli (BM41), and cohesive energies (COH41). This benchmark test set was also used to assess the performance of SCAN¹⁰ and MGGAC⁸⁰ functionals. We report the error statistics (MAE and MARE) for all the solids in TABLE III. Our benchmark calculations for the LC41 test indicate that the rMGGAC functional gives the MAE ≈ 38 mÅ, which is a remarkable improvement performance compared to MGGAC, being close to the state-of-art accuracy of the SCAN meta-GGA. We also report the MAE of the LC20 test set compiled in ref.¹⁴² for which MAEs for other methods (not included here) are also available.

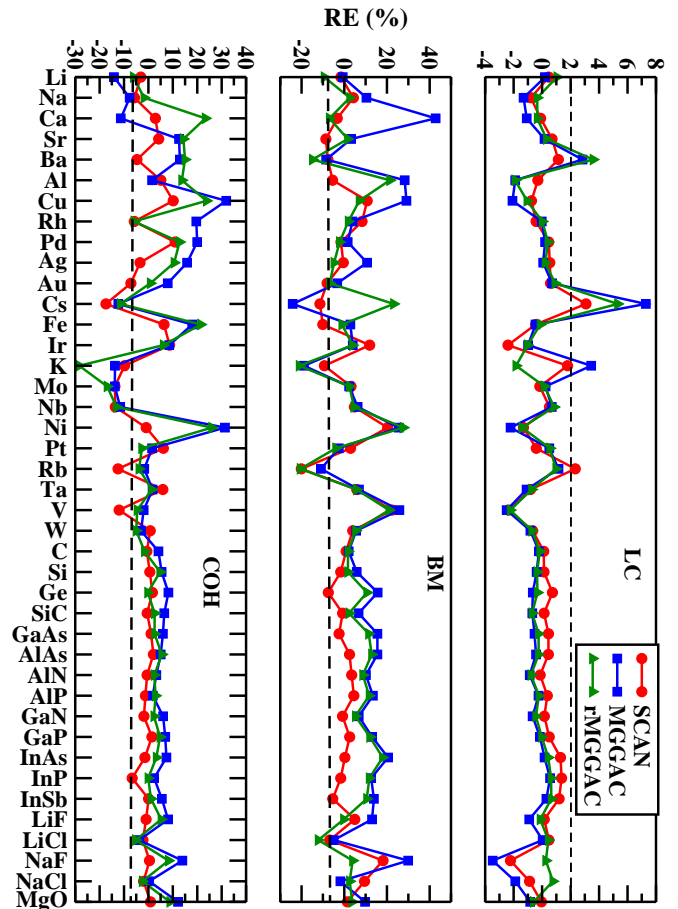


FIG. 5. Shown is the RE (%) of LC, BM, and COH test sets as obtained from different methods.

From literature we found other meta-GGAs, like the revised Tao-Perdew-Staroverov-Scuseria (revTPSS)⁶⁹ and Tao-Mo (TM)⁴⁴ semilocal functionals, that give for LC20 test, the MAE ≈ 32 mÅ^{77,142}.

The improvement of the lattice constants from rMGGAC functional is also followed by its performance for the bulk moduli, showing that the rMGGAC predicts the realistic shape of the energy versus volume curve near the equilibrium point. Thus, we obtain for the BM41 test, an improved MAE ≈ 8.5 GPa from rMGGAC compared to the MGGAC (MAE ≈ 11.5). Our benchmark values are also close to that of the SCAN where the later gives MAE of 7.5 GPa. For BM20 test set we obtain MAE of 4.6 GPa from rMGGAC. The performance of the rMGGAC for BM20 is also better or comparable than the state-of-art GGA for solids, PBEsol (MAE 6.2 GPa)¹⁴² and meta-GGA revTPSS (MAE 8.7 GPa)¹⁴² and TM (MAE 4.2 GPa)⁷⁷.

The results for the COH41 test also display the improved performance from rMGGAC (MAE of 0.30 eV/atom) over the MGGAC (MAE of 0.36 eV/atom). Here, the SCAN (MAE of 0.19 eV/atom) performs better than rMGGAC. However, our reported MAE values for COH20 indicates that rMGGAC values are close to the

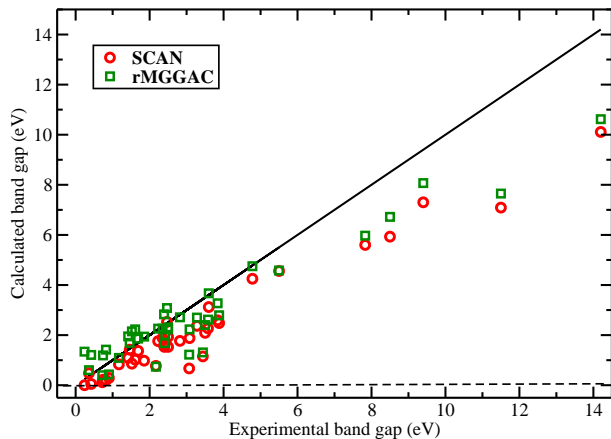


FIG. 6. Shown is the calculated versus experimental band gap for SCAN and rMGGAC functionals for 40 bulk solids considered in this work. We do not show MGGAC as its band gaps are practically same as rMGGAC.

GGA PBEsol (MAE 0.25 eV/atom)¹⁴² and TM meta-GGA semilocal functionals (MAE 0.28 eV/atom)⁷⁷. Note that for cohesive energies, well balanced performances for solids and atoms are required.

The different functional performances for the general purpose bulk solid properties are also shown in Fig. 5, where we observe an almost systematic improvement of rMGGAC over the MGGAC. For lattice constants, the Cs is challenging, for which we observe improvement from MGGAC to rMGGAC and to SCAN. Note that being a soft matter (i.e. small bulk moduli systems), the accurate description of the lattice constants of Cs needs a vdW interaction. Here, all methods overestimate the lattice constants indicating the lack of vdW interaction in the functional form. For cohesive energies and bulk moduli, we observe the magnetic Fe and Ni systems are bit of challenging for rMGGAC. Note that all these functionals overestimate the magnetic moments of the itinerant electron ferromagnets^{109,111,143-145} which is probably the source of error for bulk moduli and cohesive energies of Fe and Ni. Here, we observe that SCAN is bit better than MGGAC and rMGGAC for Ni cohesive energy.

Next, we consider the band gaps of 40 bulk semiconductors which is constructed from the 31 semiconducting band gaps of SBG31 test taken from Ref.¹³⁴, additionally we include the band gaps of 9 solids: Cu₂O, CuBr, ScN, SnTe, MgO, NaCl, LiCl, NaF, and LiF. All band gaps are calculated at the experimental lattice constants, where the lattice parameters are taken from ref.¹⁴⁶. The rMGGAC performance on band gaps of bulk solids is quite close to that of the MGGAC. Our test set consists of narrow to wide band gap insulators.

Interestingly, we observe that MGGAC and rMGGAC give non-zero band gap even for InSb, a difficult case for SCAN, where the generalized KS (gKS) gap of SCAN is zero. We obtain 1.34 eV gap for InSb from rMGGAC which is larger than the experimental reported

TABLE IV. Band gap of different solid structures (TMDC in their bulk construction and monolayers) as obtain from SCAN, MGGAC, and rMGGAC methods. For TMDC bulk the PBE spin orbit coupling (SOC) corrections (taken from Ref.⁷⁸) are subtracted from each methods. We also consider SOC corrections for monolayers.

Solids	Exp.	SCAN	MGGAC	rMGGAC
Bulk TMDC ^a				
HfS ₂	1.96	1.29	1.51	1.50
HfSe ₂	1.13	0.68	0.92	0.90
MoS ₂	1.29	1.01	1.08	1.06
MoSe ₂	1.1	0.96	1.03	1.02
WS ₂	1.35	1.18	1.16	1.14
WSe ₂	1.2	1.11	1.09	1.08
ZrS ₂	1.68	1.12	1.38	1.36
ZrSe ₂	1.2	0.51	0.80	0.76
Monolayers ^b				
h-BN	5.80 ¹⁵¹ , 6.00 ¹⁵²	4.80	5.39	5.33
MoS ₂	1.86 ¹⁵³ , 1.80 ¹⁵⁴ , 2.16 ¹⁵⁵	1.83	1.78	1.80
MoSe ₂	1.54 ¹⁵⁶ , 1.58 ¹⁵⁷ , 1.55 ¹⁵⁸	1.53	1.48	1.49
MoTe ₂	1.10 ^{159,160} , 1.02 ¹⁶¹	1.12	1.08	1.09
WS ₂	1.58 ¹⁶² , 1.57 ¹⁶³	1.71	1.85	1.87
WSe ₂	1.66 ^{164,165}	1.41	1.51	1.53
WTe ₂	1.44 ¹⁶⁶	0.73	0.79	0.81
BP	1.12 ¹⁶⁷	1.19	1.53	1.39

a) Simulations are performed at RPA calculated lattice constants^{168,169}. For reference setup and experimental values of band gaps see TABLE III of Ref.⁷⁸ and all references therein.

b) Calculated at PBE optimized lattice constants.

value (0.24 eV). The readers are suggested to go through refs.¹⁴⁷⁻¹⁴⁹ for other different functionals performance in bandgap assessments. Nevertheless, the improvement of the MGGAC and rMGGAC band gaps over SCAN method for band gap of solids within $1.5 < E_g < 6$ eV are clearly visualized from Fig. 6. The improvement in the performance of MGGAC and rMGGAC is due to the use of only α ingredient in the exchange functional form, which gives more negative slope $\partial F_x / \partial \alpha$, achieving a stronger ultra-non-locality effect⁸⁴. However, we mention that both MGGAC and rMGGAC overestimate the band gap of low-gap semiconductors, having MARE worse than SCAN.

Finally, we consider the surface energies and on top CO surface adsorption energies for (111) surfaces of transition metals Cu, Pd, Pt, Rh, and Ir. These tests are particularly interesting because they involve transition metal surface phenomena, that are important for catalytic applications. We observe that without including any van-der Waals (vdW) long-range corrections, MGGAC and rMGGAC perform slightly better than SCAN. We recall that SCAN may perform better with a vdW non-local correction^{96,150}.

C. Electronic band gap of 2D vdW Transition Metal Dichalcogenide and Monolayers

In a generalized way, 2D vdW materials offer great flexibility in terms of tuning their electronic properties^{170,171}. Thus, electronic band-gap engineering can be car-

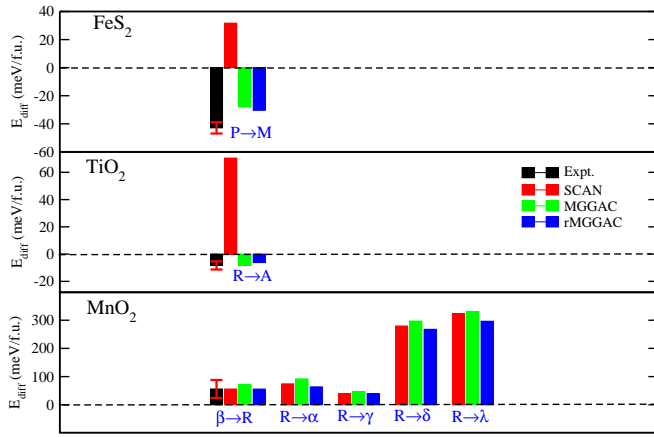


FIG. 7. Shown is the energy differences of different phases of FeS_2 , TiO_2 , and MnO_2 polymorphs. We do not consider zero-point energy (ZPE) corrections. For MnO_2 , the SCAN values are taken from reference¹⁷⁶ and MGGAC values from reference¹²⁷. For experimental values we consider enthalpy differences. Full results are also reported in Ref.¹³².

ried out by changing the number of 2D layers in a given material^{172–174}. The stacking of two or more monolayers of different vdW materials leads to the rich variety of 2D vdW quantum systems and allows researchers to explore novel and collective electronic, topological, and magnetic phenomena at the interfaces¹⁷⁵. The correlation between electron and spin, phonons, and other electrons can be significantly modulated affecting the charge transport, entropy, and total energy in the quantum limit. Especially, the bandgap engineering of 2D vdW systems from a low cost semilocal methods is still very difficult to achieve where various methods based on the hybrid density functionals and Green functional (GW) level theory is proposed. Also, the GGA functionals perform moderately to estimate the bandgaps of these systems, whereas meta-GGA methods are not vastly assessed. In the present context, we show a systematically improvable performance for bandgaps of those systems from SCAN to MGGAC and/or rMGGAC functionals. To depict this we consider bandgaps of several bulk 2D vdW transition metal dichalcogenide (TMDC) and monolayers, which are presented in Table IV. These systems have electronic band gap ranging from the semiconducting monolayer 2H-MoS₂ (1.8 eV) and black phosphorene (BP) (1.2 eV) to their bulk systems 2H-MoS₂ (1.29 eV) to wide gap insulator of hexagonal boron-nitride (h-BN) (5.4 eV). The results of the aforementioned systems are presented in TABLE IV. Inspecting TABLE IV we observe, MGGAC and rMGGAC can be considered as improved methods to address the bandgaps of the bulk TMDC to monolayer. In all the cases, the MGGAC and rMGGAC perform in a quite similar way, predicting the bandgaps better than the SCAN functional.

TABLE V. Tabulated are the phase transition pressure (P_t) (in GPa) of highly symmetric phases. The SCAN temperature corrections are added to the MGGAC and rMGGAC ground-state results. The temperature uncorrected values for all functionals are reported in Ref.¹³².

Solids	Expt. ^a	SCAN ^a	MGGAC	rMGGAC
Si	12.0	13.8	20.2	14.8
Ge	10.6	10.4	15.8	13.7
SiC	100.0	69.1	69.2	61.6
GaAs	15.0	16.1	24.1	22.9
Pb	14.0	22.2	13.7	13.1
C	3.7	8.3	7.7	6.5
BN	5.0	6.1	4.4	3.7
SiO ₂	7.5	5.2	2.0	2.6

a) See Ref.⁹⁹ and all references therein.

D. Transition pressure and structural stability

Accurate prediction of the phase transition pressure and correct ground state phase of polymorphs of solids are quite important from the point of view of the stability of the solid. Importantly, meta-GGA functionals that suffer from the order-of-limit problem, wrongly predict the phase transition pressure and structural phase transition of different polymorphs of phases^{73,177}. But functionals like SCAN and MGGAC methods do not suffer from the order-of-limit problem. In Table V, we report the phase transition pressure of different phases of the solids. We notice that the MGGAC has the tendency of overestimation the phase transition pressure for Si and Ge, while rMGGAC corrects this limitation of the MGGAC. This is because the energy differences of different phases are better described by rMGGAC than MGGAC functional. Overall, SCAN functional performs better here for all transition pressures.

The improved performance of rMGGAC is also noticeable from the structural phase stability of different polymorphs of FeS_2 , TiO_2 , and MnO_2 . These systems are known to be challenging systems for semilocal functionals as those often fail to predict the correct energy ordering of these systems^{127,176,178,179}. While the SCAN functional correctly predicts all phases of MnO_2 polymorphs, it wrongly estimates the ground states of both FeS_2 and TiO_2 . The SCAN functional predicts marcasite (M) and anatase (A) as the most stable phases over the pyrite (P) and rutile (R) phases for FeS_2 and TiO_2 , respectively^{127,178,179}. However, it is shown¹²⁷, correct energy ordering of these systems can be achieved from the MGGAC level theory. Moreover, we observe from Fig. 7 that rMGGAC further improves the performance of MGGAC in terms of the energy differences. For MnO_2 the energy differences as obtained from rMGGAC are very close or even better than those obtained using SCAN functional.

E. General thermochemical assessment

To rationalize the rMGGAC functional performance for small molecules, we consider several standard bench-

TABLE VI. MAEs (in kcal/mol) for Main group thermochemistry (MGT), Barrier heights (BH), and Non-covalent interactions (NCI) test sets. The SCAN and MGGAC values from reference⁸⁰. The SCAN and MGGAC values are taken from ref.⁸⁰.

	SCAN	MGGAC	rMGGAC
Main group thermochemistry (MGT)			
AE6 ^a	3.43	5.24	4.64
G2/148 ^b	3.73	4.38	4.61
EA13 ^c	3.22	3.16	4.14
IP13 ^d	4.43	8.04	5.73
PA8 ^e	1.41	5.59	2.74
DC9/12 ^f	11.13	6.35	11.75
HC7 ^g	6.51	4.10	6.63
BH76RC ^h	2.32	2.51	2.63
Barrier heights (BH)			
HTBH38 ⁱ	7.31	2.86	5.13
NHTBH38 ^j	7.88	4.95	5.29
Non-covalent interactions (NCI)			
HB6 ^k	0.76	0.87	0.79
DI6 ^l	0.53	0.65	0.61
PPS5 ^m	0.72	0.67	1.19
CT7 ⁿ	2.99	2.18	1.60
S22 ^o	0.92	1.20	1.61
WATER27 ^p	7.99	5.76	4.72
TMAE	4.08	3.66	3.98

(a) 6 atomization energies^{130,180,181}, (b) atomization energies of 148 molecules¹⁸², (c) electron affinity of 13 molecules¹⁸³, (d) ionization potential of 13 molecules¹⁸³, (e) 8 proton affinities¹⁸³, (f) 9 difficult cases^{180,184}, (g) 7 hydrocarbon chemistry test sets^{180,185}, (h) 30 recalculated reaction energies¹⁸⁶, (i) hydrogen transfer barrier heights of 38 molecules^{180,187}, (j) non-hydrogen transfer barrier heights of 38 molecules^{180,187}, (k) 6 hydrogen bonds^{180,188}, (l) 6 dipole interactions^{180,188}, (m) 5 $\pi - \pi$ system dissociation energies^{180,188}, (n) 7 charge transfer complexes^{180,188}, (o) 22 non-covalent interaction test set¹⁸⁹, (p) 27 water clusters binding energies^{190,191}, (q) 9 hydrogenic¹⁹², and (r) 11 non-hydrogenic molecular bonds¹⁹².

mark test cases and the results are reported in TABLE VI. The test set is divided into three subsets, namely main group thermochemistry (MGT), barrier heights (BH), and non-covalent interactions (NCI). Inspecting the performance of different methods for MGT test cases, one can immediately notice that rMGGAC improves over MGGAC for AE6, IP13 and PA8 test case. Within the other MGT test set, rMGGAC is worse than MGGAC for DC9 test set. Then, for the MGT test case, rMGGAC performs quite similarly to SCAN, and slightly worse than MGGAC. Next, for NCI test cases, we mention that rMGGAC is considerably better than MGGAC for CT7 and WATER27 test cases, for which one-electron self-interaction free correlation is important. However, for S22 and PPS5 test cases, SCAN and MGGAC perform better than rMGGAC. This is because SCAN and MGGAC better account for some amount of intermediate and short-range vdW interactions¹⁰. Finally, we mention that the performance of rMGGAC can be further enhanced for PPS5 and S22 with a long-range vdW interaction correction.

To show the impact of the rMGGAC improvement for HB6, CT7, and DI6, in Ref. 132, we also calculate the relative energy differences of the water hexamers. The deviation of the different isomers from the prism is also

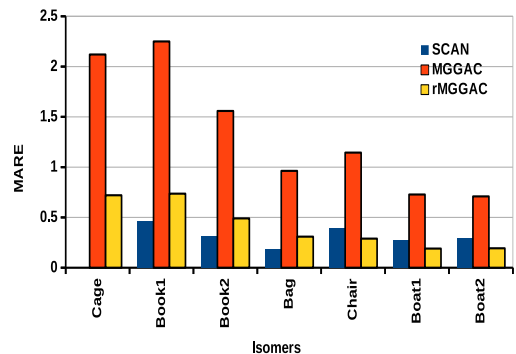


FIG. 8. MAREs of the different functionals for the water hexamers with respect to the prism isomer.

shown in Fig. 8. From Ref. 132 and Fig. 8 it is evident that all functionals correctly predict the prism isomer as the most stable water hexamer, whereas the rMGGAC significantly improves over MGGAC for the relative energies (with respect to the prism isomer) of different isomers.

IV. SUMMARY AND CONCLUDING REMARKS

We propose a revised MGGAC (rMGGAC) XC functional by combining a one-electron self-interaction free correlation functional with the original MGGAC exchange. The rMGGAC correlation functional has been constructed to satisfy important exact conditions, being exact for one-electron systems, accurate for two-electron ground-state systems, and the low- and high-density limits of the uniformly scaled density. The rMGGAC correlation energy density is smooth and without spurious structure, as shown in Fig. 1. Moreover, the rMGGAC correlation functional corrects the huge underestimation of the correlation energy of MGGAC for atoms and ions (see Table I).

The rMGGAC XC functional, as its predecessor, is an improved functional for band gap of strongly-bound solids, vdW solids, and 2D TMDC layers, but also improves considerably over MGGAC in several prospects. The performance of the rMGGAC demonstrates its successes in the broad direction of solid-state and quantum chemistry properties, which includes thermochemical, energy ordering for challenging polymorphs of solids and isomers of water hexamers, and structural properties of solids.

Lastly, we conclude that the newly designed rMGGAC functional can be further implemented to design novel materials having advance functionalities in the field of unique device architecture. Also, the rMGGAC can offer opportunities for interesting applications of advance energy storage, catalytic problems, electronics and valleytronics.

COMPUTATIONAL DETAILS

We perform molecular calculations using a development version of Q-CHEM¹⁹³ software package with def2-QZVP basis set. The XC integrals are performed with 99 points radial grid and 590 points angular Lebedev grid. Note that the present choice of the grid is adequate for the complete energy convergence of the non-bonded systems.

Solid-state calculations are performed in Vienna *Ab initio* Simulation Package (VASP)^{194–197}. For all the simulations, we use $20 \times 20 \times 20$ \mathbf{k} points sampling with energy cutoff 800 eV. For cohesive energies we consider an orthorhombic box of size $23 \times 24 \times 25 \text{ \AA}^3$ is considered. The 3^{rd} order Birch-Murnaghan equation of state is used to calculate the bulk moduli. The surface energy and CO adsorption energies are calculated with $16 \times 16 \times 1$ Γ -centered k points with an energy cutoff of 700 eV and a vacuum level of 20 \AA . For CO adsorption, we relax the top two layers.

SUPPORTING INFORMATION

The supporting information is attached with the manuscript and available online. Additional details are available to the corresponding author upon reasonable request.

ACKNOWLEDGMENTS

S.J. is grateful to the NISER for partial financial support. S.K.B acknowledges NISER for financial support. Calculations are performed in the KALINGA and NISERDFT High Performance Computing Facility, NISER. Part of the simulations and/or computations are also supported by the SAMKHYA: High Performance Computing Facility provided by Institute of Physics (IOP), Bhubaneswar. S.J. and P.S. grateful to Prof. Suresh Kumar Patra for the computational facility at IOP, Bhubaneswar. S.J. and P.S. would like to thank Q-Chem, Inc. and developers for providing the source code. S.Ś. is grateful to the National Science Centre, Poland for the financial support under Grant No. 2020/37/B/ST4/02713

Appendix A: Low density and high density limit of rMGGAC correlation functional

(a) In low density limit ($r_s \rightarrow \infty$), the rMGGAC exchange-correlation (xc) energy functional should independent of ζ for $0 \leq |\zeta| < 0.7$, a constraint important for atomization energies. In the low-density limit the LDA correlation energies behaves as,

$$\epsilon_c^{LDA0}(r_s) \rightarrow_{r_s \rightarrow \infty} -\frac{c_1}{r_s} + \frac{c_2}{r_s^{3/2}} + O(r_s^{-2}) \quad (\text{A1})$$

$$\epsilon_c^{LSDA1}(r_s, \zeta) \rightarrow_{r_s \rightarrow \infty} -\frac{d_0(\zeta)}{r_s} + \frac{d_1(\zeta)}{r_s^{3/2}} + O(r_s^{-2}) \quad (\text{A2})$$

where the coefficients related to $\epsilon_c^{LDA0}(r_s \rightarrow \infty)$ becomes $c_1 = \frac{b_{1c}}{b_{3c}}$ and $c_2 = \frac{b_{1c}b_{2c}}{b_{3c}^2}$. Similarly, we find that $d_0(\zeta)$ and $d_1(\zeta)$ becomes⁴⁹,

$$d_0(\zeta) = d_{xc}(\zeta) - \frac{3}{4\pi} \left(\frac{9\pi}{4}\right)^{1/3} d_x(\zeta), \quad (\text{A3})$$

$$d_1(\zeta) = 1.5 \quad (\text{A4})$$

where

$$d_{xc} = 0.4582d_x + 0.4335 - 0.1310f(\zeta) + 0.0262f(\zeta)\zeta^4 \quad (\text{A5})$$

and

$$d_x(\zeta) = [(1 + \zeta)^{4/3} + (1 - \zeta)^{4/3}]/2 \quad (\text{A6})$$

with $f(\zeta) = \frac{d_x - 1}{2^{1/3} - 1}$. Note that $d_1(\zeta)$ is obtained from the spin-independent coefficient from the PC model¹⁹⁸.

Finally, in the low density limit the rMGGAC correlation energy becomes,

$$\begin{aligned} W_\infty^{rMGGAC} = E_x^{MGGAC}[n_\uparrow, n_\downarrow] - \int d^3r n(\mathbf{r}) & \left[\left(\frac{c_1}{r_s} \right. \right. \\ & \left. \left. \frac{1}{[1 + 4\chi_\infty(\zeta = 0)s^2]^{1/4}} \right) G_c(\zeta) f_1(\alpha, p) \right. \\ & \left. + \left(\frac{d_0(\zeta)}{r_s} \frac{1}{[1 + 4B_1(r_s, \zeta)t^2]^{1/4}} \right) f_2(\alpha, p) \right], \end{aligned} \quad (\text{A7})$$

with $\chi_\infty(\zeta = 0) = 0.128026$, $B_1(r_s, \zeta) = \frac{\beta_0}{d_0(\zeta)} \phi(\zeta)^3 r_s$, and $t = (3\pi^2/16)^{1/3} s / (\phi(\zeta) r_s^{1/2})$. For details of the calculations and notations see main text and refs.^{10,198}.

(b) Under Levy's uniform scaling¹² to the high-density limit i.e., $n_\lambda(\mathbf{r}) = \lambda^3 n(\lambda\mathbf{r})$ with $\lambda \rightarrow \infty$ [$\lambda \rightarrow \infty$ and $r_s \rightarrow 0$] the ϵ_c^{rMGGAC} tends to

$$\epsilon_c^{rMGGAC} \rightarrow \epsilon_c^{rMGGAC-GL2} = \epsilon_c^{0GL2} f_1(\alpha, p) + \epsilon_c^{1GL2} f_2(\alpha, p), \quad (\text{A8})$$

where ϵ_c^{0GL2} and ϵ_c^{1GL2} are the Görling-Levy (GL2)^{14,22,23} limit of the correlation energy densities. Note that $f_1(\alpha, p)$ and $f_2(\alpha, p)$ remain invariant under the uniform scaling. Performing the Taylor expansion in the limit $\lambda \rightarrow \infty$ the resultant ϵ_c^{0GL2} and ϵ_c^{1GL2} are obtain as,

$$\epsilon_c^{0GL2} = b_{1c} G_c(\zeta) \ln\{1 - g_\infty(\zeta = 0, s)(\exp(1) - 1) / \exp(1)\}, \quad (\text{A9})$$

and

$$\epsilon_c^{1GL2} = \gamma \phi^3 \ln \left[1 - \frac{1}{(1 + 4\chi \frac{s^2}{\phi^2})^{1/4}} \right], \quad (\text{A10})$$

with $\chi = (\beta_0/\gamma)c^2 e^{-\omega/\gamma} \approx 0.72161$, $\beta_0 = 0.066725$, $\gamma = 0.031091$, $c = 1.2277$, and $\omega = 0.046644$. See ref.⁵⁴ for details of the parameters.

-
- * Corresponding author: subrata.jana@niser.ac.in, subrata.niser@gmail.com
 † sushant@niser.ac.in
 ‡ szsmiga@fizyka.umk.pl
 § lucian.constantin.68@gmail.com
 ¶ psamal@niser.ac.in
- ¹ W. Kohn and L. J. Sham, Phys. Rev. **140**, A1133 (1965).
 - ² A. K. Geim and I. V. Grigorieva, Nature **499**, 419 (2013).
 - ³ K. S. Novoselov, A. Mishchenko, A. Carvalho, and A. H. Castro Neto, Science **353** (2016), 10.1126/science.aac9439.
 - ⁴ J. Taylor, H. Guo, and J. Wang, Phys. Rev. B **63**, 245407 (2001).
 - ⁵ A. A. Lee, D. Vella, A. Goriely, and S. Kondrat, Phys. Rev. X **6**, 021034 (2016).
 - ⁶ A. V. Kuklin and H. Ågren, Phys. Rev. B **99**, 245114 (2019).
 - ⁷ O. V. Yazyev and M. I. Katsnelson, Phys. Rev. Lett. **100**, 047209 (2008).
 - ⁸ P. Lazić, G. M. Sipahi, R. K. Kawakami, and I. Žutić, Phys. Rev. B **90**, 085429 (2014).
 - ⁹ C. Cardoso, D. Soriano, N. A. García-Martínez, and J. Fernández-Rossier, Phys. Rev. Lett. **121**, 067701 (2018).
 - ¹⁰ J. Sun, A. Ruzsinszky, and J. P. Perdew, Phys. Rev. Lett. **115**, 036402 (2015).
 - ¹¹ M. Gmitra and J. Fabian, Phys. Rev. B **92**, 155403 (2015).
 - ¹² M. Levy and J. P. Perdew, Phys. Rev. A **32**, 2010 (1985).
 - ¹³ M. Levy, Int. J. Quantum Chem. **116**, 802 (2016).
 - ¹⁴ A. Görling and M. Levy, Phys. Rev. A **45**, 1509 (1992).
 - ¹⁵ E. Fabiano and L. A. Constantin, Phys. Rev. A **87**, 012511 (2013).
 - ¹⁶ P.-S. Svendsen and U. von Barth, Phys. Rev. B **54**, 17402 (1996).
 - ¹⁷ P. R. Antoniewicz and L. Kleinman, Phys. Rev. B **31**, 6779 (1985).
 - ¹⁸ C. D. Hu and D. C. Langreth, Phys. Rev. B **33**, 943 (1986).
 - ¹⁹ S.-K. Ma and K. A. Brueckner, Phys. Rev. **165**, 18 (1968).
 - ²⁰ P. Elliott and K. Burke, Can. J. Chem. **87**, 1485 (2009).
 - ²¹ P. Elliott, D. Lee, A. Cangi, and K. Burke, Phys. Rev. Lett. **100**, 256406 (2008).
 - ²² A. Görling and M. Levy, Phys. Rev. A **50**, 196 (1994).
 - ²³ A. Görling and M. Levy, Phys. Rev. B **47**, 13105 (1993).
 - ²⁴ A. Görling and M. Levy, Phys. Rev. A **52**, 4493 (1995).
 - ²⁵ I. Grabowski, A. M. Teale, E. Fabiano, S. Śmiga, A. Buksztel, and F. D. Sala, Molecular Physics **112**, 700 (2014), <https://doi.org/10.1080/00268976.2013.854424>.
 - ²⁶ S. Śmiga, A. Buksztel, and I. Grabowski, in *Proceedings of MEST 2012: Electronic structure methods with applications to experimental chemistry*, Advances in Quantum Chemistry, Vol. 68, edited by P. Hoggan (Academic Press, 2014) pp. 125 – 151.
 - ²⁷ A. Buksztel, S. Śmiga, and I. Grabowski, in *Electron Correlation in Molecules – ab initio Beyond Gaussian Quantum Chemistry*, Advances in Quantum Chemistry, Vol. 73, edited by P. E. Hoggan and T. Ozdogan (Academic Press, 2016) pp. 263 – 283.
 - ²⁸ S. Śmiga, I. Grabowski, M. Witkowski, B. Mussard, and J. Toulouse, Journal of Chemical Theory and Computation **16**, 211 (2020), pMID: 31816237, <https://doi.org/10.1021/acs.jctc.9b00807>.
 - ²⁹ S. Jana, S. Śmiga, L. A. Constantin, and P. Samal, Journal of Chemical Theory and Computation **16**, 7413 (2020), pMID: 33205659, <https://doi.org/10.1021/acs.jctc.0c00823>.
 - ³⁰ L. A. Constantin and J. M. Pitarke, Phys. Rev. B **83**, 075116 (2011).
 - ³¹ F. Della Sala and A. Görling, Phys. Rev. Lett. **89**, 033003 (2002).
 - ³² E. Engel, J. Chevary, L. Macdonald, and S. Vosko, Z. Phys. D **23**, 7 (1992).
 - ³³ C. M. Horowitz, L. A. Constantin, C. R. Proetto, and J. M. Pitarke, Phys. Rev. B **80**, 235101 (2009).
 - ³⁴ L. A. Constantin, E. Fabiano, J. M. Pitarke, and F. Della Sala, Phys. Rev. B **93**, 115127 (2016).
 - ³⁵ Y. M. Niquet, M. Fuchs, and X. Gonze, J. Chem. Phys. **118**, 9504 (2003).
 - ³⁶ C.-O. Almbladh and U. von Barth, Phys. Rev. B **31**, 3231 (1985).
 - ³⁷ C. J. Umrigar and X. Gonze, Phys. Rev. A **50**, 3827 (1994).
 - ³⁸ S. Śmiga, F. Della Sala, A. Buksztel, I. Grabowski, and E. Fabiano, Journal of Computational Chemistry **37**, 2081 (2016), <https://onlinelibrary.wiley.com/doi/pdf/10.1002/jcc.24436>.
 - ³⁹ S. Śmiga and L. A. Constantin, The Journal of Physical Chemistry A **124**, 5606 (2020), pMID: 32551627, <https://doi.org/10.1021/acs.jpca.0c04156>.
 - ⁴⁰ L. Pollack and J. Perdew, Journal of Physics: Condensed Matter **12**, 1239 (2000).
 - ⁴¹ A. D. Kaplan, K. Wagle, and J. P. Perdew, Phys. Rev. B **98**, 085147 (2018).
 - ⁴² L. A. Constantin, Phys. Rev. B **93**, 121104 (2016).
 - ⁴³ L. A. Constantin, Phys. Rev. B **78**, 155106 (2008).
 - ⁴⁴ J. Tao and Y. Mo, Phys. Rev. Lett. **117**, 073001 (2016).
 - ⁴⁵ J. Tao, V. N. Staroverov, G. E. Scuseria, and J. P. Perdew, Phys. Rev. A **77**, 012509 (2008).
 - ⁴⁶ J. Přecechtělová, H. Bahmann, M. Kaupp, and M. Ernzerhof, J. Chem. Phys. **141**, 111102 (2014).
 - ⁴⁷ J. P. Přecechtělová, H. Bahmann, M. Kaupp, and M. Ernzerhof, J. Chem. Phys. **143**, 144102 (2015).

- ⁴⁸ J. P. Perdew and K. Schmidt, in *AIP Conference Proceedings* (IOP INSTITUTE OF PHYSICS PUBLISHING LTD, 2001) pp. 1–20.
- ⁴⁹ J. P. Perdew and Y. Wang, *Phys. Rev. B* **45**, 13244 (1992).
- ⁵⁰ J. P. Perdew and A. Zunger, *Phys. Rev. B* **23**, 5048 (1981).
- ⁵¹ A. D. Becke, *Phys. Rev. A* **38**, 3098 (1988).
- ⁵² C. Lee, W. Yang, and R. G. Parr, *Phys. Rev. B* **37**, 785 (1988).
- ⁵³ J. P. Perdew, J. A. Chevary, S. H. Vosko, K. A. Jackson, M. R. Pederson, D. J. Singh, and C. Fiolhais, *Phys. Rev. B* **46**, 6671 (1992).
- ⁵⁴ J. P. Perdew, K. Burke, and Y. Wang, *Phys. Rev. B* **54**, 16533 (1996).
- ⁵⁵ R. Armiento and A. E. Mattsson, *Phys. Rev. B* **72**, 085108 (2005).
- ⁵⁶ Z. Wu and R. E. Cohen, *Phys. Rev. B* **73**, 235116 (2006).
- ⁵⁷ L. A. Constantin, E. Fabiano, and F. Della Sala, *Phys. Rev. B* **84**, 233103 (2011).
- ⁵⁸ Y. Zhao and D. G. Truhlar, *J. Chem. Phys.* **128**, 184109 (2008).
- ⁵⁹ L. A. Constantin, A. Terentjevs, F. Della Sala, and E. Fabiano, *Phys. Rev. B* **91**, 041120 (2015).
- ⁶⁰ E. Fabiano, L. A. Constantin, and F. Della Sala, *Int. J. Quantum Chem.* **113**, 673 (2013).
- ⁶¹ L. A. Constantin, A. Ruzsinszky, and J. P. Perdew, *Phys. Rev. B* **80**, 035125 (2009).
- ⁶² A. Cancio, G. P. Chen, B. T. Krull, and K. Burke, *J. Chem. Phys.* **149**, 084116 (2018).
- ⁶³ A. Albavera-Mata, K. Botello-Mancilla, S. B. Trickey, J. L. Gázquez, and A. Vela, *Phys. Rev. B* **102**, 035129 (2020).
- ⁶⁴ A. D. Becke and M. R. Roussel, *Phys. Rev. A* **39**, 3761 (1989).
- ⁶⁵ T. Van Voorhis and G. E. Scuseria, *J. Chem. Phys.* **109**, 400 (1998).
- ⁶⁶ Y. Zhao and D. G. Truhlar, *J. Chem. Phys.* **125**, 194101 (2006).
- ⁶⁷ J. P. Perdew, S. Kurth, A. c. v. Zupan, and P. Blaha, *Phys. Rev. Lett.* **82**, 2544 (1999).
- ⁶⁸ J. Tao, J. P. Perdew, V. N. Staroverov, and G. E. Scuseria, *Phys. Rev. Lett.* **91**, 146401 (2003).
- ⁶⁹ J. P. Perdew, A. Ruzsinszky, G. I. Csonka, L. A. Constantin, and J. Sun, *Phys. Rev. Lett.* **103**, 026403 (2009).
- ⁷⁰ L. A. Constantin, E. Fabiano, and F. Della Sala, *J. Chem. Theory Comput.* **9**, 2256 (2013).
- ⁷¹ J. Sun, R. Haunschuld, B. Xiao, I. W. Bulik, G. E. Scuseria, and J. P. Perdew, *J. Chem. Phys.* **138**, 044113 (2013).
- ⁷² J. Sun, J. P. Perdew, and A. Ruzsinszky, *Proc. Natl. Acad. Sci. U. S. A.* **112**, 685 (2015).
- ⁷³ A. Ruzsinszky, J. Sun, B. Xiao, and G. I. Csonka, *J. Chem. Theory Comput.* **8**, 2078 (2012).
- ⁷⁴ H. S. Yu, X. He, and D. G. Truhlar, *Journal of Chemical Theory and Computation* **12**, 1280 (2016), pMID: 26722866, <https://doi.org/10.1021/acs.jctc.5b01082>.
- ⁷⁵ Y. Wang, X. Jin, H. S. Yu, D. G. Truhlar, and X. He, *Proc. Natl. Acad. Sci. U. S. A.* **114**, 8487 (2017).
- ⁷⁶ P. D. Mezei, G. I. Csonka, and M. Kállay, *J. Chem. Theory Comput.* **14**, 2469 (2018).
- ⁷⁷ S. Jana, K. Sharma, and P. Samal, *The Journal of Physical Chemistry A* **123**, 6356 (2019).
- ⁷⁸ B. Patra, S. Jana, L. A. Constantin, and P. Samal, *Phys. Rev. B* **100**, 045147 (2019).
- ⁷⁹ A. Patra, S. Jana, H. Myneni, and P. Samal, *Phys. Chem. Chem. Phys.* **21**, 19639 (2019).
- ⁸⁰ B. Patra, S. Jana, L. A. Constantin, and P. Samal, *Phys. Rev. B* **100**, 155140 (2019).
- ⁸¹ S. Śmiga, E. Fabiano, L. A. Constantin, and F. Della Sala, *J. Chem. Phys.* **146**, 064105 (2017).
- ⁸² J. W. Furness and J. Sun, *Phys. Rev. B* **99**, 041119 (2019).
- ⁸³ J. W. Furness, A. D. Kaplan, J. Ning, J. P. Perdew, and J. Sun, *The Journal of Physical Chemistry Letters* **11**, 8208 (2020).
- ⁸⁴ T. Aschebrock and S. Kümmel, *Phys. Rev. Research* **1**, 033082 (2019).
- ⁸⁵ P. Haas, F. Tran, and P. Blaha, *Phys. Rev. B* **79**, 085104 (2009).
- ⁸⁶ F. Tran, J. Stelzl, and P. Blaha, *J. Chem. Phys.* **144**, 204120 (2016).
- ⁸⁷ S. Śmiga, E. Fabiano, S. Laricchia, L. A. Constantin, and F. Della Sala, *The Journal of Chemical Physics* **142**, 154121 (2015), <https://doi.org/10.1063/1.4917257>.
- ⁸⁸ S. Śmiga, E. Fabiano, L. A. Constantin, and F. Della Sala, *The Journal of Chemical Physics* **146**, 064105 (2017), <https://doi.org/10.1063/1.4975092>.
- ⁸⁹ Z.-h. Yang, H. Peng, J. Sun, and J. P. Perdew, *Phys. Rev. B* **93**, 205205 (2016).
- ⁹⁰ H. Peng, Z.-H. Yang, J. P. Perdew, and J. Sun, *Phys. Rev. X* **6**, 041005 (2016).
- ⁹¹ Y. Mo, R. Car, V. N. Staroverov, G. E. Scuseria, and J. Tao, *Phys. Rev. B* **95**, 035118 (2017).
- ⁹² G. Tian, Y. Mo, and J. Tao, *Computation* **5** (2017), 10.3390/computation5020027.
- ⁹³ G. Tian, Y. Mo, and J. Tao, *J. Chem. Phys.* **146**, 234102 (2017).
- ⁹⁴ Y. Mo, G. Tian, and J. Tao, *Chem. Phys. Lett.* **682**, 38 (2017).
- ⁹⁵ Y. Mo, G. Tian, and J. Tao, *Phys. Chem. Chem. Phys.* **19**, 21707 (2017).
- ⁹⁶ A. Patra, J. E. Bates, J. Sun, and J. P. Perdew, *Proceedings of the National Academy of Sciences* **114**, E9188 (2017), <https://www.pnas.org/content/114/44/E9188.full.pdf>.
- ⁹⁷ H. Peng and J. P. Perdew, *Phys. Rev. B* **96**, 100101 (2017).
- ⁹⁸ Y. Zhang, J. Sun, J. P. Perdew, and X. Wu, *Phys. Rev. B* **96**, 035143 (2017).
- ⁹⁹ N. Sengupta, J. E. Bates, and A. Ruzsinszky, *Phys. Rev. B* **97**, 235136 (2018).
- ¹⁰⁰ C. Shahi, J. Sun, and J. P. Perdew, *Phys. Rev. B* **97**, 094111 (2018).
- ¹⁰¹ H. Tang and J. Tao, *Materials Research Express* **5**, 076302 (2018).
- ¹⁰² Y. Mo, H. Tang, A. Bansil, and J. Tao, *AIP Advances* **8**, 095209 (2018).
- ¹⁰³ S. Jana, A. Patra, and P. Samal, *J. Chem. Phys.* **149**, 044120 (2018).
- ¹⁰⁴ S. Jana, K. Sharma, and P. Samal, *J. Chem. Phys.* **149**, 164703 (2018).
- ¹⁰⁵ A. Patra, S. Jana, and P. Samal, *J. Phys. Chem. A* **123**, 10582 (2019).
- ¹⁰⁶ A. Patra, H. Peng, J. Sun, and J. P. Perdew, *Phys. Rev. B* **100**, 035442 (2019).
- ¹⁰⁷ S. Jana, L. A. Constantin, and P. Samal, *Journal of Chemical Theory and Computation* **16**, 974 (2020).
- ¹⁰⁸ A. Patra, S. Jana, L. A. Constantin, and P. Samal, *The*

- Journal of Chemical Physics **153**, 084117 (2020).
- ¹⁰⁹ D. Mejía-Rodríguez and S. B. Trickey, Phys. Rev. B **102**, 121109 (2020).
- ¹¹⁰ Y. Zhang, W. Zhang, and D. J. Singh, Phys. Chem. Chem. Phys. **22**, 19585 (2020).
- ¹¹¹ F. Tran, G. Baudesson, J. Carrete, G. K. H. Madsen, P. Blaha, K. Schwarz, and D. J. Singh, Phys. Rev. B **102**, 024407 (2020).
- ¹¹² Y. Wang, P. Verma, L. Zhang, Y. Li, Z. Liu, D. G. Truhlar, and X. He, Proceedings of the National Academy of Sciences **117**, 2294 (2020), <https://www.pnas.org/content/117/5/2294.full.pdf>.
- ¹¹³ J. Sun, B. Xiao, Y. Fang, R. Haunschild, P. Hao, A. Ruzsinszky, G. I. Csonka, G. E. Scuseria, and J. P. Perdew, Phys. Rev. Lett. **111**, 106401 (2013).
- ¹¹⁴ J. Tao, J. P. Perdew, V. N. Staroverov, and G. E. Scuseria, Phys. Rev. Lett. **91**, 146401 (2003).
- ¹¹⁵ M. Levy and H. Ou-Yang, Physical Review A **38**, 625 (1988).
- ¹¹⁶ A. Holas and N. March, Physical Review A **44**, 5521 (1991).
- ¹¹⁷ K. Finzel and M. Kohout, Theoretical Chemistry Accounts **137**, 1 (2018).
- ¹¹⁸ S. Śmiga, S. Sicińska, and E. Fabiano, Phys. Rev. B **101**, 165144 (2020).
- ¹¹⁹ L. A. Constantin, Phys. Rev. B **99**, 155137 (2019).
- ¹²⁰ J. Sun, R. Haunschild, B. Xiao, I. W. Bulik, G. E. Scuseria, and J. P. Perdew, J. Chem. Phys. **138**, 044113 (2013).
- ¹²¹ J. Wellendorff, K. T. Lundgaard, K. W. Jacobsen, and T. Bligaard, J. Chem. Phys. **140**, 144107 (2014).
- ¹²² E. H. Lieb and S. Oxford, Int. J. Quantum Chem. **19**, 427 (1981).
- ¹²³ J. P. Perdew, A. Ruzsinszky, J. Sun, and K. Burke, J. Chem. Phys. **140**, 18A533 (2014).
- ¹²⁴ J. W. Furness, N. Sengupta, J. Ning, A. Ruzsinszky, and J. Sun, The Journal of Chemical Physics **152**, 244112 (2020), <https://doi.org/10.1063/5.0008014>.
- ¹²⁵ A. D. Becke and M. R. Roussel, Phys. Rev. A **39**, 3761 (1989).
- ¹²⁶ A. Patra, B. Patra, L. A. Constantin, and P. Samal, Phys. Rev. B **102**, 045135 (2020).
- ¹²⁷ B. Patra, S. Jana, L. A. Constantin, and P. Samal, J. Phys. Chem. C (Accepted) (2021).
- ¹²⁸ J. P. Perdew, K. Burke, and M. Ernzerhof, Phys. Rev. Lett. **77**, 3865 (1996).
- ¹²⁹ J. Sun, J. P. Perdew, Z. Yang, and H. Peng, J. Chem. Phys. **144**, 191101 (2016).
- ¹³⁰ R. Haunschild and W. Klopper, Theor. Chem. Acc. **131**, 1112 (2012).
- ¹³¹ J. P. Perdew, J. Tao, V. N. Staroverov, and G. E. Scuseria, J. Chem. Phys. **120**, 6898 (2004).
- ¹³² Supplementary Material.
- ¹³³ L. A. Constantin, Phys. Rev. B **99**, 085117 (2019).
- ¹³⁴ P. Verma and D. G. Truhlar, J. Phys. Chem. Lett. **8**, 380 (2017).
- ¹³⁵ N. R. Kestner and O. Sinanoğlu, Phys. Rev. **128**, 2687 (1962).
- ¹³⁶ C. Filippi, C. J. Umrigar, and M. Taut, The Journal of Chemical Physics **100**, 1290 (1994), <https://doi.org/10.1063/1.466658>.
- ¹³⁷ S. Kais, D. R. Herschbach, N. C. Handy, C. W. Murray, and G. J. Laming, The Journal of Chemical Physics **99**, 417 (1993), <https://doi.org/10.1063/1.465765>.
- ¹³⁸ S. Śmiga and L. A. Constantin, Journal of Chemical Theory and Computation **16**, 4983 (2020), PMID: 32559078, <https://doi.org/10.1021/acs.jctc.0c00328>.
- ¹³⁹ S. Jana, B. Patra, S. Śmiga, L. A. Constantin, and P. Samal, Phys. Rev. B **102**, 155107 (2020).
- ¹⁴⁰ E. Matito, J. Cioslowski, and S. F. Vyboishchikov, Phys. Chem. Chem. Phys. **12**, 6712 (2010).
- ¹⁴¹ L. A. Constantin, E. Fabiano, and F. Della Sala, Journal of Chemical Theory and Computation **9**, 2256 (2013), PMID: 26583719, <https://doi.org/10.1021/ct400148r>.
- ¹⁴² J. Sun, M. Marsman, G. I. Csonka, A. Ruzsinszky, P. Hao, Y.-S. Kim, G. Kresse, and J. P. Perdew, Phys. Rev. B **84**, 035117 (2011).
- ¹⁴³ D. Mejía-Rodríguez and S. Trickey, Phys. Rev. B **98**, 115161 (2018).
- ¹⁴⁴ D. Mejía-Rodríguez and S. Trickey, Phys. Rev. B **100**, 041113 (2019).
- ¹⁴⁵ Y. Fu and D. J. Singh, Phys. Rev. Lett. **121**, 207201 (2018).
- ¹⁴⁶ F. Tran and P. Blaha, J. Phys. Chem. A **121**, 3318 (2017).
- ¹⁴⁷ F. Tran, J. Doumont, L. Kalantari, A. W. Huran, M. A. L. Marques, and P. Blaha, Journal of Applied Physics **126**, 110902 (2019), <https://doi.org/10.1063/1.5118863>.
- ¹⁴⁸ P. Borlido, T. Aull, A. W. Huran, F. Tran, M. A. L. Marques, and S. Botti, Journal of Chemical Theory and Computation **15**, 5069 (2019), PMID: 31306006, <https://doi.org/10.1021/acs.jctc.9b00322>.
- ¹⁴⁹ P. Borlido, J. Schmidt, A. W. Huran, F. Tran, M. A. L. Marques, and S. Botti, npj Computational Materials **6**, 96 (2020).
- ¹⁵⁰ S. Mallikarjun Sharada, R. K. B. Karlsson, Y. Maimaiti, J. Voss, and T. Bligaard, Phys. Rev. B **100**, 035439 (2019).
- ¹⁵¹ S. Okada, M. Igami, K. Nakada, and A. Oshiyama, Phys. Rev. B **62**, 9896 (2000).
- ¹⁵² F. Paleari, T. Galvani, H. Amara, F. Ducastelle, A. Molina-Sánchez, and L. Wirtz, 2D Materials **5**, 045017 (2018).
- ¹⁵³ T. Eknapakul, P. D. C. King, M. Asakawa, P. Buaphet, R.-H. He, S.-K. Mo, H. Takagi, K. M. Shen, F. Baumberger, T. Sasagawa, S. Jungthawan, and W. Meevasana, Nano Letters **14**, 1312 (2014).
- ¹⁵⁴ D. Jena and A. Konar, Phys. Rev. Lett. **98**, 136805 (2007).
- ¹⁵⁵ M. M. Ugeda, A. J. Bradley, S.-F. Shi, F. H. da Jornada, Y. Zhang, D. Y. Qiu, W. Ruan, S.-K. Mo, Z. Hussain, Z.-X. Shen, F. Wang, S. G. Louie, and M. F. Crommie, Nature Materials **13**, 1091 (2014).
- ¹⁵⁶ B. K. Choi, M. Kim, K.-H. Jung, J. Kim, K.-S. Yu, and Y. J. Chang, Nanoscale Research Letters **12**, 492 (2017).
- ¹⁵⁷ Y. Zhang, T.-R. Chang, B. Zhou, Y.-T. Cui, H. Yan, Z. Liu, F. Schmitt, J. Lee, R. Moore, Y. Chen, H. Lin, H.-T. Jeng, S.-K. Mo, Z. Hussain, A. Bansil, and Z.-X. Shen, Nature Nanotechnology **9**, 111 (2014).
- ¹⁵⁸ S. Tongay, J. Zhou, C. Ataca, K. Lo, T. S. Matthews, J. Li, J. C. Grossman, and J. Wu, Nano Letters **12**, 5576 (2012).
- ¹⁵⁹ C. Ruppert, O. B. Aslan, and T. F. Heinz, Nano Letters **14**, 6231 (2014).
- ¹⁶⁰ I. G. Lezama, A. Arora, A. Ubaldini, C. Barreateau, E. Gi-

- annini, M. Potemski, and A. F. Morpurgo, *Nano Letters* **15**, 2336 (2015).
- ¹⁶¹ I. G. Lezama, A. Ubaldini, M. Longobardi, E. Gianini, C. Renner, A. B. Kuzmenko, and A. F. Morpurgo, *2D Materials* **1**, 021002 (2014).
- ¹⁶² B. Amin, T. P. Kaloni, and U. Schwingenschlögl, *RSC Adv.* **4**, 34561 (2014).
- ¹⁶³ F. Zhang, Y. Lu, D. S. Schulman, T. Zhang, K. Fujisawa, Z. Lin, Y. Lei, A. L. Elias, S. Das, S. B. Sinnott, and M. Terrones, *Science Advances* **5** (2019).
- ¹⁶⁴ W.-T. Hsu, L.-S. Lu, D. Wang, J.-K. Huang, M.-Y. Li, T.-R. Chang, Y.-C. Chou, Z.-Y. Juang, H.-T. Jeng, L.-J. Li, and W.-H. Chang, *Nature Communications* **8**, 929 (2017).
- ¹⁶⁵ E. Blundo, M. Felici, T. Yildirim, G. Pettinari, D. Tedeschi, A. Miriametro, B. Liu, W. Ma, Y. Lu, and A. Polimeni, *Phys. Rev. Research* **2**, 012024 (2020).
- ¹⁶⁶ V. Dixit, C. Vyas, V. M. Pathak, G. K. Soalanki, and K. D. Patel, *AIP Conference Proceedings* **1953**, 070020 (2018).
- ¹⁶⁷ Z. Huisheng, Y. Wenjia, N. Yaohui, and X. Xiaohong, *Nanoscale* **12**.
- ¹⁶⁸ T. Björkman, A. Gulans, A. V. Krasheninnikov, and R. M. Nieminen, *Phys. Rev. Lett.* **108**, 235502 (2012).
- ¹⁶⁹ T. Björkman, *The Journal of Chemical Physics* **141**, 074708 (2014), <https://doi.org/10.1063/1.4893329>.
- ¹⁷⁰ C. H. Choi, S. H. Park, and S. I. Woo, *ACS Nano* **6**, 7084 (2012).
- ¹⁷¹ J. Wang, J. Hao, D. Liu, S. Qin, D. Portehault, Y. Li, Y. Chen, and W. Lei, *ACS Energy Letters* **2**, 306 (2017).
- ¹⁷² Z.-S. Wu, A. Winter, L. Chen, Y. Sun, A. Turchanin, X. Feng, and K. Müllen, *Advanced Materials* **24**, 5130 (2012).
- ¹⁷³ C. Zhao, Z. Xu, H. Wang, J. Wei, W. Wang, X. Bai, and E. Wang, *Advanced Functional Materials* **24**, 5985 (2014).
- ¹⁷⁴ A. Du, *Wiley Interdisciplinary Reviews: Computational Molecular Science* **6**, 551 (2016).
- ¹⁷⁵ T. B. Martins, R. H. Miwa, A. J. R. da Silva, and A. Fazzio, *Phys. Rev. Lett.* **98**, 196803 (2007).
- ¹⁷⁶ D. A. Kitchaev, H. Peng, Y. Liu, J. Sun, J. P. Perdew, and G. Ceder, *Phys. Rev. B* **93**, 045132 (2016).
- ¹⁷⁷ A. Patra, S. Jana, and P. Samal, *The Journal of Chemical Physics* **153**, 184112 (2020), <https://doi.org/10.1063/5.0025173>.
- ¹⁷⁸ M.-Y. Zhang, Z.-H. Cui, and H. Jiang, *J. Mater. Chem. A* **6**, 6606 (2018).
- ¹⁷⁹ Z.-H. Cui, F. Wu, and H. Jiang, *Phys. Chem. Chem. Phys.* **18**, 29914 (2016).
- ¹⁸⁰ R. Peverati and D. G. Truhlar, *Philos. Trans. R. Soc., A* **372** (2014).
- ¹⁸¹ B. J. Lynch and D. G. Truhlar, *J. Phys. Chem. A* **107**, 8996 (2003).
- ¹⁸² L. A. Curtiss, P. C. Redfern, K. Raghavachari, and J. A. Pople, *J. Chem. Phys.* **109**, 42 (1998).
- ¹⁸³ R. Peverati and D. G. Truhlar, *Philos. Trans. R. Soc. London A* **372**, 20120476 (2014).
- ¹⁸⁴ R. Peverati and D. G. Truhlar, *J. Chem. Theory Comput.* **8**, 2310 (2012).
- ¹⁸⁵ R. Peverati, Y. Zhao, and D. G. Truhlar, *J. Phys. Chem. Lett.* **2**, 1991 (2011).
- ¹⁸⁶ L. Goerigk, A. Hansen, C. Bauer, S. Ehrlich, A. Najibi, and S. Grimme, *Phys. Chem. Chem. Phys.* **19**, 32184 (2017).
- ¹⁸⁷ A. Karton, A. Tarnopolsky, J.-F. Lamère, G. C. Schatz, and J. M. L. Martin, *J. Phys. Chem. A* **112**, 12868 (2008).
- ¹⁸⁸ Y. Zhao and D. G. Truhlar, *J. Chem. Theory Comput.* **3**, 289 (2007).
- ¹⁸⁹ J. Jurečka, J. Šponer, J. Černý, and P. Hobza, *Phys. Chem. Chem. Phys.* **8**, 1985 (2006).
- ¹⁹⁰ V. S. Bryantsev, M. S. Diallo, A. C. T. van Duin, and W. A. Goddard, *J. Chem. Theory Comput.* **5**, 1016 (2009).
- ¹⁹¹ D. Manna, M. K. Kesharwani, N. Sylvetsky, and J. M. L. Martin, *J. Chem. Theory Comput.* **13**, 3136 (2017).
- ¹⁹² Y. Zhao and D. G. Truhlar, *J. Chem. Phys.* **125**, 194101 (2006).
- ¹⁹³ Y. e. a. Shao, *Mol. Phys.* **113**, 184 (2015).
- ¹⁹⁴ G. Kresse and J. Hafner, *Phys. Rev. B* **47**, 558 (1993).
- ¹⁹⁵ G. Kresse and J. Furthmüller, *Phys. Rev. B* **54**, 11169 (1996).
- ¹⁹⁶ G. Kresse and D. Joubert, *Phys. Rev. B* **59**, 1758 (1999).
- ¹⁹⁷ G. Kresse and J. Furthmüller, *Comput. Mater. Sci.* **6**, 15 (1996).
- ¹⁹⁸ M. Seidl, J. P. Perdew, and S. Kurth, *Phys. Rev. A* **62**, 012502 (2000).